Journal of Magnetism and Magnetic Materials 321 (2009) 1351–1355

Contents lists available at ScienceDirect

Journal of Magnetism and Magnetic Materials

journal homepage: www.elsevier.com/locate/jmmm

Dipolar chains formed by chemically synthesized cobalt nanocubes

Guangjun Cheng [a,*], Robert D. Shull [b], A.R. Hight Walker [a]

[a] Optical Technology Division, Physics Laboratory, National Institute of Standards and Technology (NIST), Gaithersburg, MD 20899-8443, United States
[b] Metallurgy Division, Materials Science and Engineering Laboratory, NIST, Gaithersburg, MD 20899-8552, United States

ARTICLE INFO

Available online 20 February 2009

Keywords:
Cobalt
Nanocubes
Magnetic nanoparticles
Dipolar chains
Magnetic property

ABSTRACT

Cobalt nanocubes with an average edge length of 50 nm and epsilon crystalline structure were synthesized via thermo-decomposition in 1,2-dichlorobenzene at 120 °C in the presence of surfactants. These nanocubes form dipolar chains upon drying in zero applied field and bundles of chains along the direction of an applied magnetic field. The magnetic measurements reveal strong interparticle couplings among the nanocubes in their dried magnetic-field-induced assemblies. The constricted hysteresis loops and near-zero coercivity indicate the existence of vortex states in the assemblies. Exposure to electron beam heats up the nanocubes and turns the dipolar chains into nanowires.

Magnetic nanocubes and their assemblies possess unique properties due to their size, shape and surface effects [1,2]. In nature, magnetite nanocubes and their assemblies are found in magnetotactic bacteria [3,4] and minerals [5]. With recent advancements in the wet-chemical synthesis of magnetic nanoparticles with controllable sizes and shapes, several magnetic nanocubes including iron [6,7], iron oxides [8], iron–platinum [9], and manganese ferrite [10] have been synthesized. In the case of cobalt (Co) nanoparticles, although the synthesis and characterization of spherical nanoparticles and nanodisks have been well investigated [11–16], there are only few reports on Co nanocubes [13,17]. Ref. [13] briefly mentioned that, in comparison with the synthesis of the spherical Co nanoparticles, Co nanocubes can be obtained by lowering the reaction temperature to 100 °C. Ref. [17] reported on the synthesis and magnetic properties of Co nanocubes, which were prepared by wet-chemistry, but these nanocubes were a mixture of hexagonal close packed (hcp) Co and ε–Co [17]. In this paper, we report on the synthesis and characterization of single phase ε–Co nanocubes and their assemblies. We are particularly interested in the formation of dipolar chains by these nanocubes with and without an external magnetic field.

Co nanocubes were synthesized via thermo-decomposition in 1,2-dichlorobenzene (DCB) at 120 °C in the presence of trioctylphosphine oxide (TOPO). Transmission electron microscopy (TEM) was used to characterize the morphology of the as-prepared nanocubes and their assemblies, while X-ray diffraction (XRD) was used to characterize their crystalline structure. A superconducting quantum interference device (SQUID) magnetometer was used to characterize their magnetic properties.

In contrast to the conventional thermo-decomposition method for synthesizing monodisperse spherical Co nanoparticles [11–16], here, the reaction temperature is much lower and fewer surfactants are used for the synthesis of the Co nanocubes. Typically, tri-octylphosphine oxide (0.05 g, TOPO, 90%, Alfa Aesar, Ward Hill, MA) and di-cobalt octa-carbonyl (0.5 g, $Co_2(CO)_8$, containing 1–5% hexane as a stabilizer, Alfa Aesar, Ward Hill, MA) were degassed in argon in a flask for 20 min. Then, 10 mL of 1,2-dichlorobenzene (DCB, 99%, anhydrous, Aldrich, Milwaukee, WI) was introduced into the flask under an argon atmosphere. The solution was heated to 120 °C. The reaction continued for another 30 min and then the black colloids were extracted using an air-tight syringe and stored in a glass vial under argon.

Fig. 1 shows the TEM images and XRD pattern of the as-prepared Co nanoparticles. TEM samples were prepared by dropping the colloids onto a carbon-coated TEM grid (Formvar/Carbon Cu grids, Ted Pella, Inc. Redding, CA) and allowing the DCB to evaporate in air. TEM images were obtained on a HITACHI H-600 microscope operated at 100 kV. Powder X-ray diffraction was performed using a Phillips diffractometer. The pattern was collected at ambient temperature using Cu Kα radiation. The sample was prepared by depositing the concentrated black colloids onto a glass slide and allowing the sample to dry in air.

As we can see from the TEM image in Fig. 1a, most of the as-prepared Co nanoparticles have a square projection shape and a few nanoparticles have a hexagonal one. These nanoparticles are poly-disperse and have a wide size distribution. The average edge length of the squares is determined to be 50 nm with 15 nm standard deviation. In order to accurately confirm the three-dimensional structure of the as-prepared Co nanoparticles, the TEM grid was tilted with respect to the plane perpendicular to the

* Corresponding author. Tel.: +301 975 5209; fax: +301 975 6991.
E-mail address: guangjun.cheng@nist.gov (G. Cheng).

0304-8853/$ - see front matter © 2009 Elsevier B.V. All rights reserved.
doi:10.1016/j.jmmm.2009.02.037

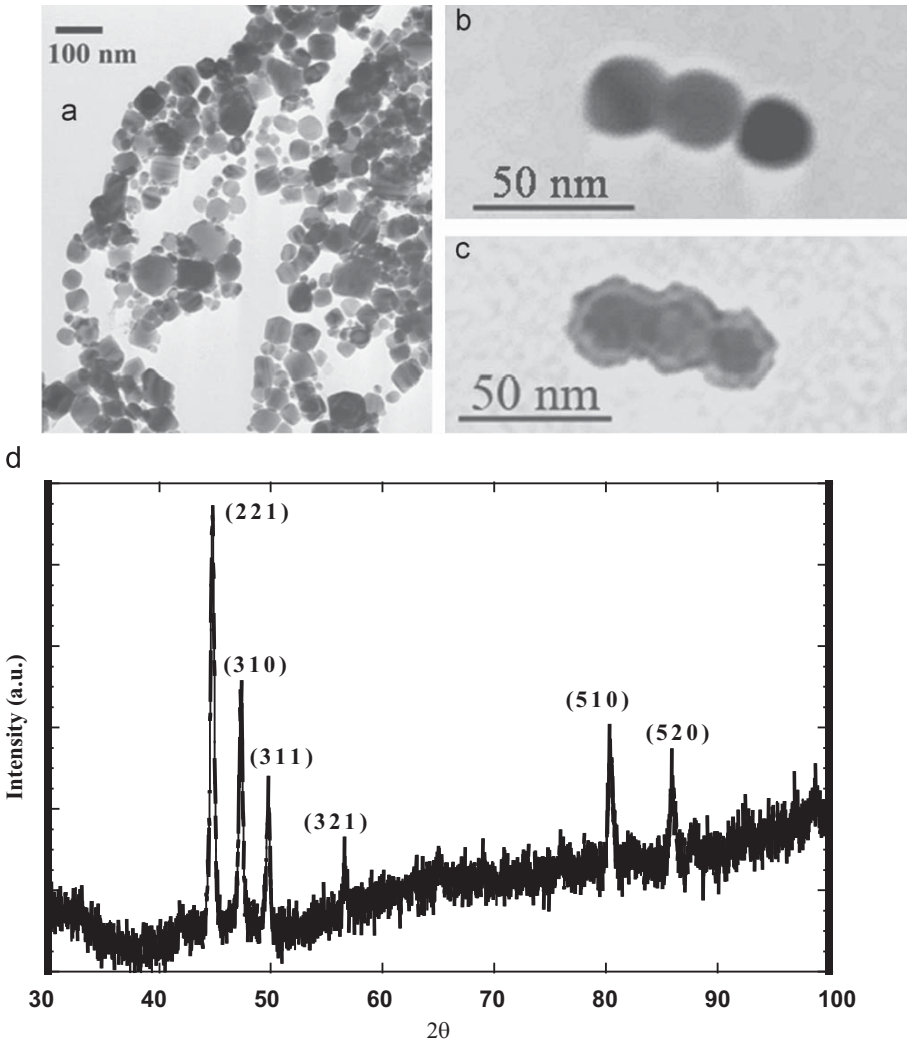

Fig. 1. Characterization of Co nanocubes: (a) and (b) TEM images, (c) TEM image of (b) after sample tilting, and (d) XRD pattern measured at room temperature.

electron beam. Fig. 1b presents a TEM image of three Co nanoparticles standing side by side prior to tilting. After the TEM sample was tilted with an angle of 25°, the TEM image in Fig. 1c shows that the projection shape of three nanoparticles changed to hexagonal. This is a clear indication that the as-prepared Co nanoparticles are nanocubes [18]. Also, after sample titling, the thickness of the tilted nanocubes will not be uniform as shown in Fig. 1c. In this figure, the contrast variation due to the thickness difference can clearly be observed [19]. An XRD pattern of the as-prepared Co nanocubes is shown in Fig. 1d. All of the diffraction peak positions match well with the ones for ε–Co [11–16]. No peaks for hcp or faced-centered cubic (fcc) Co nor peaks for Co oxides are observed in this XRD pattern. Therefore, no detectable hcp or fcc Co are produced here and no significant oxidation occurs for these as-prepared nanocubes.

In the presence of strong dipolar interactions, magnetic nanoparticles dispersed in a liquid carrier tend to form the dipolar chains even without an external applied magnetic field [15,16,20,21]. Measurements using conventional TEM and cryogenic TEM have demonstrated the growing effect of dipolar attractions as the size of the magnetite particles increases [21]. Fig. 2a shows that Co nanocubes formed a single-particle dipolar chain on a TEM grid upon drying in zero applied field. In this single-particle dipolar chain, the Co nanocubes in the middle of the chain are close packed with two opposite cubic faces interacting with their neighbors. This chain is similar to the magnetite nanoparticle chain found in magnetotactic bacteria [3]. However, in comparison with the well-defined space between the nanoparticles in the magnetite chain, some of Co nanocubes appear to be in close contact with their neighbors due to the fewer surfactants and much stronger interactions between the cubic faces.

Our earlier work demonstrated the formation of magnetic-field-induced (MFI) assemblies by spherical Co nanoparticles [15]. Fig. 2b shows a TEM image of the MFI bundles of chains formed by Co nanocubes. The TEM sample was prepared by dropping the colloids onto a TEM grid. Then a magnet (Fisher Scientific, Pittsburgh, PA) with a 0.05 T magnetic field strength was placed near the edge of the TEM grid. MFI chains will form along the direction of the external magnetic field. The sample was allowed to dry under ambient conditions. The TEM image in Fig. 2b clearly shows two parallel, micron-sized, bundles of chains.

A superconducting quantum interference device magnetometer (SQUID, Quantum Design MPMS) was used to measure

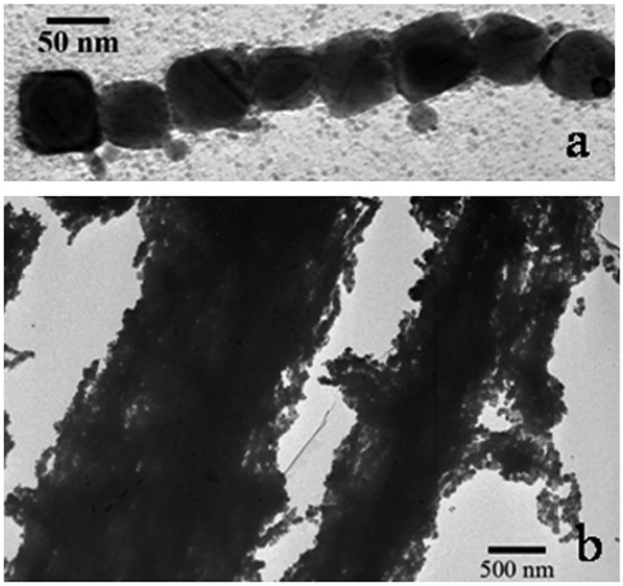

Fig. 2. TEM images of (a) a single-particle dipolar chain of Co nanocubes in zero applied field and (b) magnetic-field-induced bundles of chains.

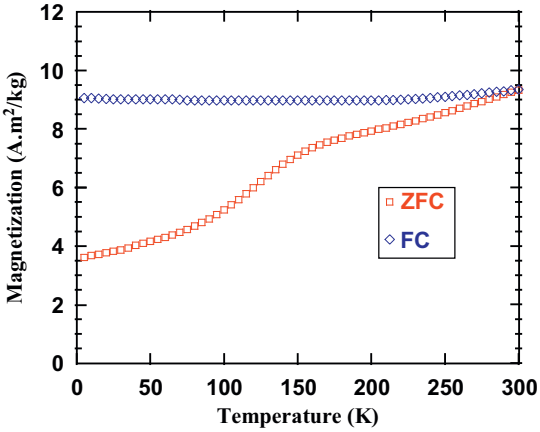

Fig. 3. ZFC/FC magnetization measurements of Co nanocubes as a function of temperature with an external magnetic field strength of 15.9 kA/m (200 Oe).

the magnetic properties of the as-prepared Co nanocubes. The sample was prepared by placing the colloids in a gelatin capsule, attracting the Co nanocubes to the bottom using a magnet, extracting the solvent, and blowing the sample dry with argon. Upon drying, the Co nanocubes stuck to the inner wall of the sample holder and prevented further physical movement in the dried sample. Presumably, the MFI assemblies of Co nanocubes will be retained in the sample holder during drying. The magnetic properties of the dried assemblies were characterized through the measurements of zero-field cooled/field cooled (ZFC/FC) magnetization as a function of temperature and hysteresis loops. For ZFC/FC magnetization measurements, the sample was first cooled to 5 K in the absence of the external magnetic field and then a 15.9 kA/m (200 Oe) external magnetic field was applied. The magnetization data were recorded during warming from 5 to 300 K as ZFC measurements. The FC measurements were performed after the ZFC measurements. The magnetizations were recorded when the sample was cooled from 300 to 5 K in the applied magnetic field.

The measurements of ZFC/FC magnetization as a function of temperature have been widely used to investigate the superparamagnetism of non-interacting single-domain nanoparticles or the super-ferromagnetism of interacting single-domain nanoparticles [1]. Fig. 3 shows ZFC/FC magnetization measurements as a function of temperature for Co nanocubes. At 15.9 kA/m (200 Oe), a gradual increase in the magnetization is observed in the ZFC curve as the temperature increases from 5 to 150 K, and afterwards the magnetization keeps increasing at a relatively slow pace until the temperature reaches 300 K. During warming, thermal energy is provided gradually to align the magnetic moments of the Co nanocubes with the field. As the temperature decreases from 300 to 5 K in the FC curve, the magnetization changes only slightly. The interparticle couplings among the Co nanocubes keep the alignment of these magnetic moments with the field. Here, ZFC/FC magnetization data clearly suggest a collective behavior in the dried MFI assemblies and strong interparticle couplings among the Co nanocubes [16].

For hysteresis loops, a +1.59 MA/m (+20 kOe) field was applied to saturate the sample, and then the magnetization was recorded as the field decreased to −1.59 MA/m (−20 kOe) and then increased to +1.59 MA/m (+20 kOe). The hysteresis loops were measured first at 5 K and then at 300 K. The saturation magnetization value was determined to be 111 A m^2/kg at 5 K and 107 A m^2/kg at 300 K, which is significantly lower than the saturation magnetization value of 162 A m^2/kg at 300 K for bulk hcp Co [17]. This lower value of saturation magnetization is probably due to the combination of a different crystalline structure of the Co nanocubes, the presence of many small particles which have not saturated at the highest field, and probably also a small amount of surface oxidation.

Fig. 4a and b show the central part of the hysteresis loops of the dried MFI assemblies for field strengths between −159 and +159 kA/m (−2 and +2 kOe) measured at 5 and 300 K, respectively. Compared with the hysteresis loops for spherical Co nanoparticles [15], the hysteresis loops for Co nanocubes have a distinct difference.

The hysteresis loops at both 5 and 300 K for the Co nanocubes are constricted when the applied field approaches zero. For example, as shown in the red curve in Fig. 4a, when the applied magnetic field decreases to 2.38 kA/m (30 Oe), the magnetization slowly decreases to 41.1 A m^2/kg, and then as the applied magnetic field approaches to zero, the magnetization experiences a sudden drop to 13.6 A m^2/kg. When the applied field direction is reversed, only a small coercivity is observed, 2 kA/m (25 Oe). The magnetization experiences a sudden increase in magnitude from −0.26 to −27.6 A m^2/kg as the applied field changes from −2.4 to −6.4 kA/m (−30 to −80 Oe), and then the magnetization magnitude starts to increase gradually. Similar behavior was also observed in the reverse curve in Fig. 4a as the magnetic field changes from −1.59 (−20 kOe) to +1.59 MA/m (−20 to +20 kOe). At 300 K, the hysteresis loop in Fig. 4b exhibits similar behavior with a smaller hysteresis area.

A constricted hysteresis loop shape can indicate the existence of a vortex state [22]. The sudden loss of magnetization near zero field is indicative of the formation of a flux closure structure. In the literature, vortex states have been reported in circular nanomagnets [23]. The study on the magnetic properties of deep, submicron circular nanomagnets as a function of both diameter and thickness has shown that as the diameter and thickness of nanomagnets decrease, vortex states are replaced by single-domain states [23]. It has also been reported that magnetite nanocubes act collectively and form magnetic superstates wherein several neighboring single-domain nanocubes arrange their magnetization vectors to form a closed circle [5]. These vortex states were observed directly using off-axis electron holography in

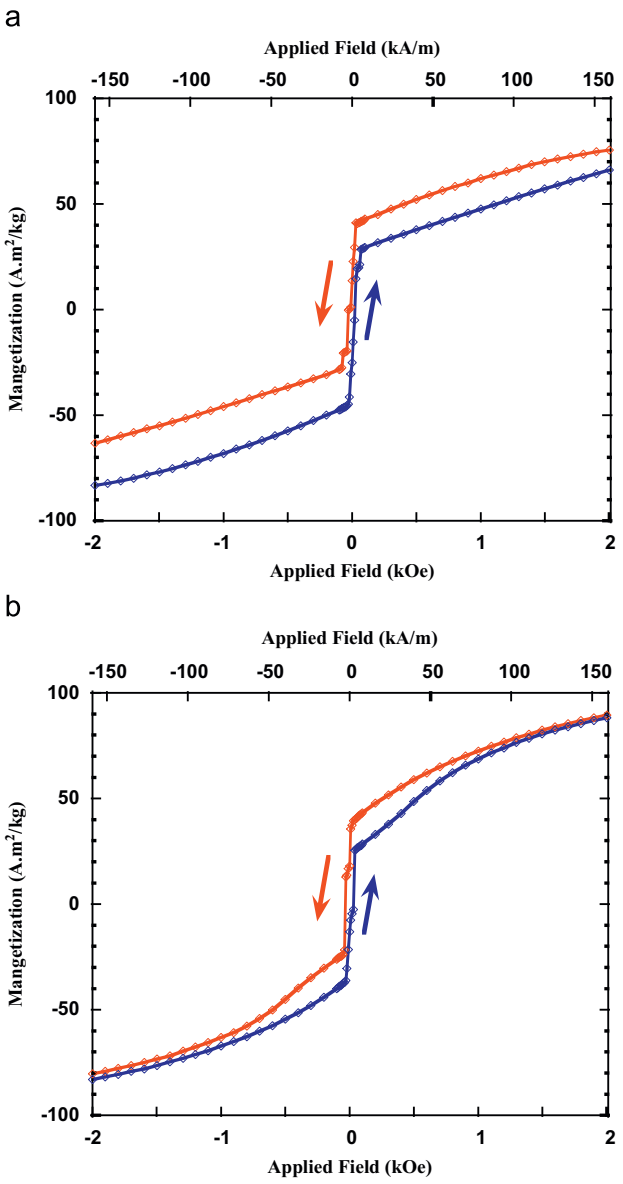

Fig. 4. Central part of hysteresis loops of Co nanocubes measured at (a) 5 K and (b) 300 K.

the transmission electron microscope. It was estimated that 50 nm is the maximum single-domain size for spherical Co nanoparticles [1]. Here, we have cobalt nanocubes with an average size of 50 nm. These nanocubes in the dried MFI assemblies act collectively and form vortex states. The fact that the hysteresis loops show a discontinuous drop in the magnetization magnitude when the external magnetic field is reduced to a critical low value indicates the vortex states, which possess zero magnetization, form very quickly. This quick formation suggests the interparticle interactions among the Co nanocubes are very strong.

The as-prepared Co nancubes also exhibit instability under electron beam irradiation. Fig. 5a shows a TEM image of the dipolar chains formed by Co nanocubes supported on a carbon-coated Cu TEM grid. Here, the nanocubes are intact and maintain their cubic shape. However, under the same imaging condition, as the electron beam keeps illuminating the sample, the Co

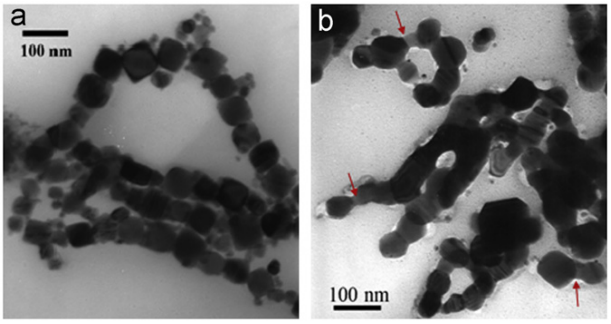

Fig. 5. TEM images of (a) dipolar chains of intact Co nanocubes and (b) Co nanowires formed by melting Co nanocubes after 3 min exposure to electron beam irradiation. These two images were not taken in the same area.

nanocubes start to melt and lose their sharp corners and edges. As shown in Fig. 5b, after a three-minute exposure, the Co nanocubes lose their well-defined cubic edges and melt together with their neighbors. The dipolar chains turn into nanowires. Also, as indicated by the arrows in Fig. 5b, for those nanocubes that are not in close contact with each other, a "bridge" forms between the nanocubes to facilitate the conversion of dipolar chains into nanowires.

The electron beam can strongly interact with a specimen. A high-energy electron loses part of its energy via inelastic scattering in the specimen and generates heat. An investigation on melting of submicron aluminum–silicon (Al–Si) alloy particles under electron beam irradiation has shown that a temperature increase caused by electron beam irradiation and poor thermal conduction away from the particle are responsible for the melting of particles well below the actual melting temperature [24]. It was also reported that, in metallic nanowires, the electron beam induces rapid local surface melting and enhanced surface diffusion, in addition to local vaporization [25].

However, we never observe melting of 10 nm spherical Co nanoparticles under the same electron beam irradiation. These much smaller nanoparticles appear more stable than those nanocubes. Here, for these nanocubes in close contact with their neighbors on TEM grids, heat from the electron beam cannot efficiently dissipate away from their sharp corners, and the neighboring Co nanocubes melt together, resulting in the formation of nanowires. However, these nanocubes do not just melt collectively. We also observe bridge formation for those nanocubes not in close contact with each other. For individual nanocubes, melting is probably initiated at the sharp corners and edges where thermal conduction of heat is not fast. Compared with the spherical nanoparticles synthesized at 180 °C, these nanocubes are synthesized at 120 °C. When the reaction temperature rises or the reaction time increases, these nanocubes form a black film on the sidewall of the reaction flask, suggesting thermal instability of the as-prepared nanocubes.

In conclusion, we have synthesized Co nanocubes in DCB at 120 °C via thermo-decomposition using TOPO as surfactants. The as-prepared nanocubes have an average edge length of 50 nm and epsilon crystalline structure. In zero applied field, these nanocubes form single-particle chains upon drying on a TEM grid. An external magnetic field induces the formation of bundles of chains along the field direction. For the dried MFI assemblies of Co nanocubes, the ZFC/FC magnetization measurements as a function of temperature reveal strong interparticle couplings among the nanocubes. Due to the collective behavior in the assemblies, these nanocubes form vortex states, as shown by their constricted hysteresis loops. Under electron beam irradiation, the as-prepared

nanocubes melt and the nanoparticle chains turn into nanowires. These studies not only provide fundamental understanding of the shape effect of nanoparticles on their magnetic properties and the collective behavior in their assemblies, but also pave a way for exploring their biological applications in magnetic resonance imaging and hyperthermia treatment.

We acknowledge the help of Mr. Tiejun Zhang at the University of Maryland, College Park for TEM measurements. We thank Ms. Rosetta V. Drew (Materials Science and Engineering Laboratory, NIST) for her help with SQUID measurements and Dr. Igor Levin (Materials Science and Engineering Laboratory, NIST) for his help with XRD measurements.

Disclaimer: We identify certain commercial equipment, instruments, or materials in this article to specify adequately the experimental procedure. In no case does such identification imply recommendation or endorsement by the National Institute of Standards and Technology, nor does it imply that the materials or equipment identified are necessarily the best available for the purpose.

References

[1] S.A. Majetich, M. Sachan, J. Phys. D: Appl. Phys. 39 (2006) R407.
[2] S. Yamamuro, K. Sumiyama, Chem. Phys. Lett. 418 (2006) 166.
[3] R.E. Dunin-Borkowski, M.R. McCartney, R.B. Frankel, et al., Science 282 (1998) 1868.
[4] J.M. Thomas, E.T. Simpson, T. Kasama, R.E. Dunin-Borkowski, Acc. Chem. Res. 41 (2008) 665.
[5] R.J. Harrison, R.E. Dunin-Borkowski, A. Putnis, Proc. Natl. Acad. Sci. USA 99 (2002) 16556.
[6] F. Dumestre, B. Chaudret, C. Amiens, et al., Science 303 (2004) 821.
[7] J. Park, K. An, Y. Hwang, et al., Nat. Mater. 3 (2004) 891.
[8] F.X. Redl, C.T. Black, G.C. Papaefthymiou, et al., J. Am. Chem. Soc. 126 (2004) 14583.
[9] M. Chen, J. Kim, J.P. Liu, et al., J. Am. Chem. Soc. 128 (2006) 7132.
[10] H. Zeng, P.M. Rice, S.X. Wang, S. Sun, J. Am. Chem. Soc. 126 (2004) 11458.
[11] V.F. Puntes, K.M. Krishnan, A.P. Alivisatos, Science 291 (2001) 2115.
[12] V.F. Puntes, D. Zanchet, C. Erdonmenz, A.P. Alivisatos, J. Am. Chem. Soc. 124 (2002) 12874.
[13] V.F. Puntes, K.M. Krishnan, A.P. Alivisatos, Top. Catal. 19 (2002) 145.
[14] G. Cheng, J.D. Carter, T. Guo, Chem. Phys. Lett. 400 (2004) 122.
[15] G. Cheng, D. Romero, G.T. Fraser, A.R. Hight Walker, Langmuir 21 (2005) 12055.
[16] G. Cheng, C.L. Dennis, R.D. Shull, A.R. Hight Walker, Langmuir 23 (2007) 11740.
[17] C.P. Gräf, R. Birringer, A. Michels, Phys. Rev. B 73 (2006) 212401.
[18] Y. Xiong, J. Ye, X. Gu, Q.-W. Chen, J. Phys. Chem. C 111 (2007) 6998.
[19] D.B. Williams, C.B. Carter, Transmission Electron Microscopy III, Imaging, Plenum Press, New York, 1996.
[20] K. Butter, P.H.H. Bomans, P.M. Frederik, et al., Nat. Mater. 2 (2003) 88.
[21] M. Klokkenburg, C. Vonk, E.M. Claesson, et al., J. Am. Chem. Soc. 126 (2004) 16706.
[22] J. Sort, A. Hoffmann, S.-H. Chung, et al., Phys. Rev. Lett. 95 (2005) 67201.
[23] R.P. Cowburn, D.K. Koltsov, A.O. Adeyeye, et al., Phys. Rev. Lett. 83 (1999) 1042.
[24] T. Yokota, M. Murayama, J.M. Howe, Phys. Rev. Lett. 91 (2003) 265504.
[25] S. Xu, M. Tian, J. Wang, et al., Small 1 (2005) 1221.